BIOCHEMISTRY
including biophysical chemistry & molecular biology

Article

pubs.acs.org/biochemistry

Changes in Protein Dynamics of the DNA Repair Dioxygenase AlkB upon Binding of Fe^{2+} and 2-Oxoglutarate

Boris Bleijlevens,*[,†,‡] Tara Shivarattan,[†] Kim S. van den Boom,[§] Annett de Haan,[‡] Gert van der Zwan,[§] Pete J. Simpson,[†] and Steve J. Matthews*[,†]

[†]Division of Molecular Biosciences, Faculty of Natural Sciences, Imperial College London, South Kensington Campus, London SW7 2AZ, U.K.

[‡]Department of Medical Biochemistry, Academic Medical Center, University of Amsterdam, Meibergdreef 15, 1105 AZ Amsterdam, The Netherlands

[§]Biomolecular Analysis and Spectroscopy, LaserLab, Vrije Universiteit Amsterdam, De Boelelaan 1081, 1081 HV, The Netherlands

Supporting Information

ABSTRACT: The *Escherichia coli* DNA repair enzyme AlkB is a 2-oxoglutarate (2OG)-dependent Fe^{2+} binding dioxygenase that removes methyl lesions from DNA and RNA. To date, nine human AlkB homologues are known: ABH1 to ABH8 and the obesity-related FTO. Similar to AlkB, these homologues exert their activity on nucleic acids, although for some homologues the biological substrate remains to be identified. 2OG dioxygenases require binding of the cofactors Fe^{2+} and 2OG in the active site to form a catalytically competent complex. We present a structural analysis of AlkB using NMR, fluorescence, and CD spectroscopy to show that AlkB is a dynamic protein exhibiting different folding states. In the absence of the cofactors Fe^{2+} and 2OG, apoAlkB is a highly dynamic protein. Binding of either Fe^{2+} or 2OG alone does not significantly affect the protein dynamics. Formation of a fully folded and catalytically competent holoAlkB complex only occurs when both 2OG and Fe^{2+} are bound. These findings provide the first insights into protein folding of 2OG-dependent dioxygenases. A role for protein dynamics in the incorporation of the metal cofactor is discussed.

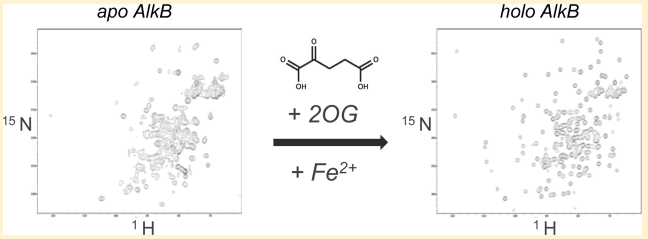

The genetic information encoded on DNA is continuously at risk of being damaged by both endogenous and exogenous factors. Alkylating agents constitute a large class of DNA damaging agents that generate both mutagenic and cytotoxic DNA lesions. In *Escherichia coli* the detrimental effects of alkylation are counteracted via the adaptive response.[1] The adaptive response results in increased expression of proteins that promote survival by counteracting certain types of DNA methylation damage. One of these proteins is AlkB, an iron-dependent oxidoreductase and member of the diverse family of 2-oxoglutarate (2OG)-dependent dioxygenases. This versatile enzyme family comprises enzymes that act on a wide range of substrates including proteins, lipids, and nucleic acids.[2] AlkB catalyzes the demethylation of 1-methyladenine and 3-methylcytosine coupled to the oxidative decarboxylation of 2OG to succinate and CO_2.[3,4] Hydroxylation of the methyl group causes a destabilization of the lesion and promotes its release as formate. Besides DNA, methylated RNA was also found to be an AlkB substrate, representing the first documented observation of relatively efficient RNA repair.[5,6] Homologues of AlkB have been identified across species ranging from bacteria to man, with at least nine human homologues documented: ABH1−8 and FTO.[7] Similar to AlkB, all nine homologues contain the essential 2OG and Fe^{2+} binding domains. Despite the low overall sequence identity, members of this family are predicted to contain similar secondary structure elements that fold into a double-stranded β-helix (DSBH) domain. To date, three homologues (ABH1, ABH2, and ABH3) have been identified as *bona fide* DNA/RNA repair enzymes.[5,8,9] ABH8 has been identified as a methyltransferase using tRNA as a substrate.[10] In addition, genome wide association studies (GWAs) have shown FTO to be associated with obesity.[11] Like AlkB, FTO also displays DNA/RNA demethylase activity, at least *in vitro*.[12,13]

Crystal structures of AlkB and its human homologues ABH2, ABH3, ABH8, and FTO have revealed that the canonical DSBH domain is very well conserved in this subfamily of 2OG dioxygenases.[14−17] The DSBH comprises a large β-sheet (formed by β-strands C1, C8, C3, and C6) and a smaller β-sheet (C2, C7, C4, and C5), sandwiching the metal and cofactor binding pocket. Two highly conserved regions in the DSBH can be distinguished: the metal-binding region, which contains the H_{131}-D_{133}-H_{187} metal-coordinating triad presented by the minor β-sheet, and the 2OG-binding N_{120}-R_{204}-R_{210} motif in the major β-sheet (AlkB residue numbering). The

Received: November 11, 2011
Revised: March 20, 2012
Published: March 26, 2012

crystal structures further show that 2OG essentially forms a molecular bridge, connecting the DSBH's major and minor sheets. The 1-carboxylate and 2-oxo functionality of 2OG coordinate the metal ion, presented by the minor sheet, in a bidentate manner. The 2OG moiety further connects to the major sheet via two additional contacts. The 5-carboxylate end of 2OG interacts with the major sheet via hydrogen bonding with the side chains of residues R204 and R210. In addition, the 2OG 1-carboxylate forms a hydrogen bond with the side chain of residue N120 in the major sheet.[18] Essentially, these interactions via 2OG and metal hold the central part of the DSBH together. The DSBH core is supported by two N-terminal α-helices and a third, smaller β-sheet that acts as a substrate-binding lid. DNA binds to AlkB via a multitude of contacts between the nucleotide backbone phosphates and the protein. The X-ray structure of AlkB in complex with double-stranded DNA displayed even more contacts anchoring the dsDNA backbone phosphate groups alongside the methylated base.[15] The methylated base is flipped out relative to the flanking bases and stacked in a hydrophobic cavity between residues Trp69 and His131 with its methyl group pointing toward the active site Fe^{2+} ion.

We have shown before that binding of 2OG or succinate to AlkB changes the protein dynamics.[18] None of the crystallographic studies on AlkB or other members of the 2OG dioxygenase family have previously shown substantial changes in protein dynamics or folding.[19] In the current study we present evidence that the apo form of AlkB is a molten globule-like dynamic ensemble of preformed secondary structure elements. We further describe the effects of cofactor and metal binding on the folding state of AlkB. These data provide a first example of how protein folding occurs in 2OG dioxygenases. These data further present a picture of AlkB as an intrinsically flexible protein, the dynamics of which might be essential for efficient catalytic repair of methyl lesions on nucleic acids.

EXPERIMENTAL PROCEDURES

Protein Expression and Purification. Recombinant *E. coli* AlkB was purified essentially as described before.[20] Briefly, C-terminally His_6-tagged AlkB was cloned in a pET21b expression vector (Novagen). Recombinant AlkB was overexpressed in *E. coli* BL21 (DE3) and purified over a Ni-NTA column mounted on an ÄKTA-Prime purification system (GE Healthcare). Bound protein was eluted using an imidazole gradient. Protein purity was checked by SDS-PAGE. Control experiments were performed on AlkB cloned into a pET30a expression vector (Novagen). This construct contained a cleavable His_6-tag. See Supporting Information for details.

NMR Experiments. NMR data were recorded on a Bruker Avance 500 MHz spectrometer equipped with a pulse field gradient triple-resonance cryoprobe. 2D $^{1}H-^{15}N$ HSQC spectra were recorded at 310 K using 150 μM protein samples in 50 mM Tris-HCl buffer at pH 7.6. HoloAlkB was prepared by subsequent addition of 1 mM 2OG and 250 μM $FeSO_4$ in the presence of 50 mM DTT. Spectra were analyzed using NMRViewJ (One Moon Scientific).

Equilibrium Fluorescence Spectroscopy. Fluorescence emission spectra were recorded on a Perkin-Elmer LS-55 fluorescence spectrophotometer equipped with a pulsed xenon source. Samples were measured in a stirred 10 × 4 mm quartz cuvette equilibrated at 20 °C. Excitation wavelength was 295 nm; emission spectra were recorded from 310 to 420 at 1 nm resolution (data collection 0.5 s/data point). Slit widths for excitation and emission were 5 nm. Spectra were recorded at an AlkB concentration of 1 μM in 20 mM Tris-HCl, pH 7.6, containing 150 mM NaCl. Fluorescence anisotropy data were collected under similar conditions but using a 5 × 5 mm quartz cuvette (Hellma). Presented anisotropy data are averages of at least 10 readings in duplicate experiments. Thermal denaturation of AlkB complexes was monitored by fluorescence signal intensity similar to above. Sample temperature was controlled via a PTP-1 Fluorescence Peltier System (Perkin-Elmer). The signal intensity was monitored at 443 nm using an excitation slit width of 5 nm and an emission slit width of 6 nm. AlkB concentration was 0.5 μM.

Time-Resolved Fluorescence Decay Spectroscopy. Tryptophan lifetimes were measured using the time-correlated single photon counting (TCSPC) technique. Samples were excited with 3 ps laser pulses at a wavelength of 295 nm, and fluorescence decays were measured over a range of wavelengths spanning the emission spectrum of tryptophan every 10 nm. The instrumental response time was ~15 ps. Deconvoluted traces were fitted with three lifetimes using a Levenbergh–Marquardt-based nonlinear fitting routine. Decay times were found to be virtually independent of the emission wavelength, and decay associated spectra (DAS) were constructed using the amplitudes of the fit. Reconstructed emission spectra from these data sets were found to be in excellent agreement with steady-state emission spectra. A full description of the experimental TCSPC setup and data analysis can be found in ref 21. Sample concentrations were AlkB 7 μM, Fe^{2+} 10 μM, NOG 1 mM in 20 mM Tris-HCl, pH 7.6.

Circular Dichroism. Spectra were recorded on a Chirascan CD spectrometer (Applied Photophysics). Far-UV CD spectra were recorded from 180 to 300 nm in a 1 mm path length quartz cuvette (Hellma) at 20 °C at a concentration of 12.5 μM (0.3 mg/mL) AlkB in 1 mM Tris-HCl, pH 7.6. Spectra were collected for 0.5 s per data point at 0.5 nm step size (spectral bandwidth 1 nm) and were corrected for background signals from buffer and/or cofactors. Spectral deconvolution using the DICHROWEB server (http://www.cryst.bbk.ac.uk/cdweb) provided estimates for secondary structure content.[22] The CSSTR algorithm was used to fit the spectra on the basis of two different reference data sets (set 4 and set 7), in the wavelength range 190–260 nm. Both sets produced similar results with good fits (NRMSD < 0.05).

Near-UV CD spectra were recorded from 240 to 360 nm. Samples (1 mg/mL in 20 mM Tris-HCl, pH 7.6) were measured in a 4 × 10 mm quartz cuvette, 4 mm path length (Hellma). Data were collected for 2 s per data point at 0.5 nm step size (spectral bandwidth 1 nm). Presented data are averages of three scans. Samples were cooled to 10 °C during recording. Spectra were corrected for background signals. To prevent auto-oxidation of holoAlkB,[23] the catalytically inert cobalt complexes were used to record near-UV CD spectra.

RESULTS

Protein conformational dynamics of AlkB complexes were assessed by NMR spectroscopy. Recombinant His_6-tagged AlkB was overexpressed in *E. coli* and affinity-purified over a Ni-NTA column. In the course of the purification, EDTA was added to remove adventitiously bound metals. During this procedure Fe^{2+} was also removed from the active site resulting in the purification of inactive apo protein. Catalytically active holoAlkB was prepared by addition of both Fe^{2+} (equimolar

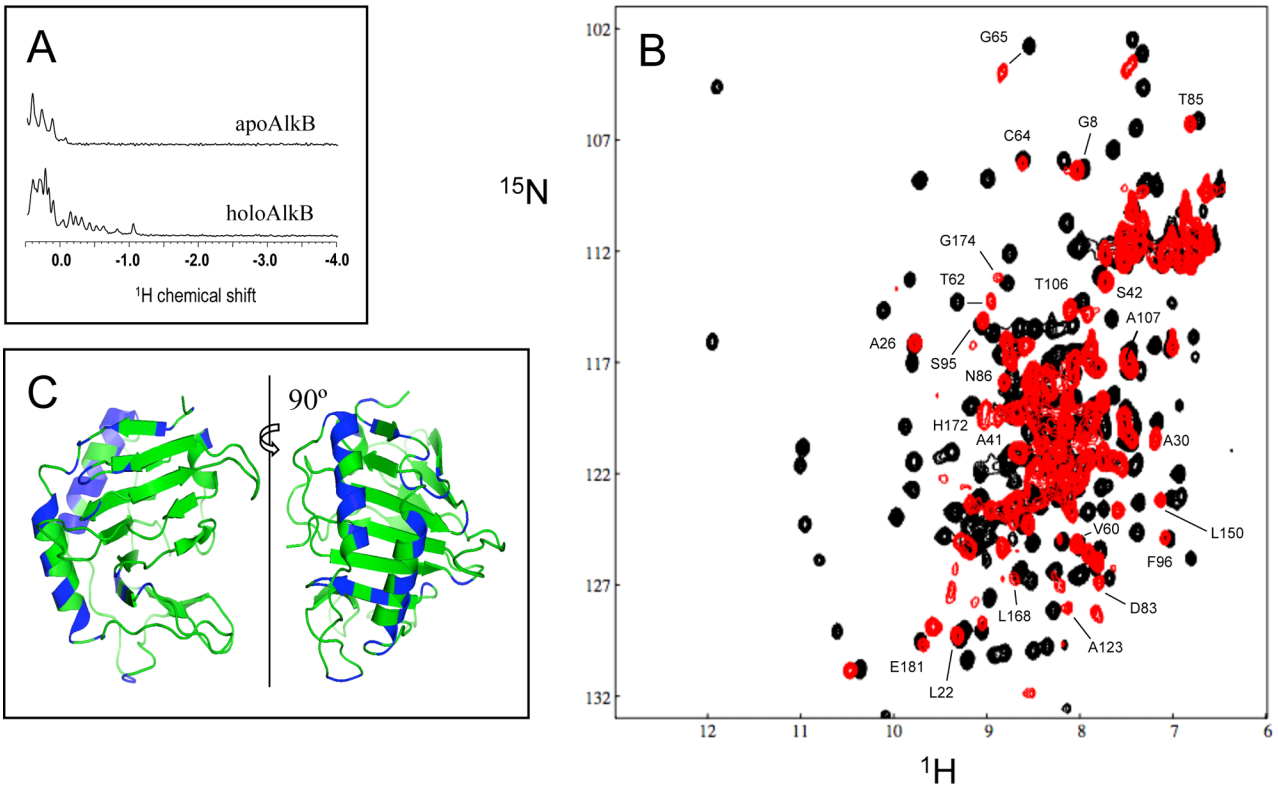

Figure 1. Folding of AlkB monitored by NMR spectroscopy. (A) ^{1}H 1D spectra of apo- and holoAlkB. An expansion of the upfield methyl region is shown for clarity. (B) ^{1}H−^{15}N 2D HSQC NMR spectra of apoAlkB (red) and holoAlkB: AlkB-Fe^{2+}-2OG (black). Tentative assignments based on a "nearest-neighbor" approach are indicated. (C) Tentatively assigned residues (in blue) are mapped on the crystal structure of holoAlkB (PDB 2FD8). For reasons of clarity, only the protein backbone is displayed, and the active site Fe^{2+} and 2OG as well as the bound oligonucleotide have been omitted. The picture was produced using MacPyMOL (DeLano Scientific, 2006).

amounts metal-to-protein) and 2OG (10−100-fold excess) to apo protein under reducing conditions (50 mM DTT). HoloAlkB displayed resolved resonances in the upfield region of the 1D ^{1}H NMR spectrum (between 0.5 and −1.5 ppm), indicative of a well-folded, globular protein (Figure 1A). Signals in this region of the NMR spectrum are typically derived from methyl groups packed against aromatic side chains in the folded, hydrophobic regions of a protein. Increased dispersion and sharpening of these signals is consistent with formation of a rigidly tumbling domain. Folding of holoAlkB protein was also apparent from the number of resonances in the 2D ^{15}N−^{1}H HSQC spectrum of the AlkB-Fe^{2+}-2OG complex (Figure 1B). A total of 182 resonances in the HSQC spectrum of holoAlkB were assigned to specific residues (BMRB entry 6685).[24] The AlkB pET21b construct used in this study consists of 224 amino acids (see Supporting Information for details). The protein contains 18 proline residues that do not give rise to signals in ^{1}H−^{15}N HSQC spectra.

In comparison with holoAlkB, apoAlkB gave rise to a 1D ^{1}H NMR spectrum that was characterized by fewer peaks in the upfield methyl region (Figure 1A), implying the absence of a significant hydrophobic core. The absence of a large number of resonances in the 2D ^{15}N−^{1}H HSQC spectrum further supported this notion (Figure 1B). The ^{15}N−^{1}H HSQC spectrum of apoAlkB showed poor spectral dispersion and significantly fewer resonances than expected for a globular protein of 224 residues. A tentative "nearest-neighbor" assignment allowed for the identification of only 23 resonances in apoAlkB. Most of these residues mapped to the α-helices supporting the DSBH (indicated in blue in Figure 1C), suggesting that at least this part of the apo protein is structurally similar to the holo complex. Most other resonances were broadened beyond detection or were shifted to such an extend that they could not be assigned to a particular residue. However, in the absence of cofactors the protein is also not completely unfolded or random coil as indicated by the absence of sharp resonances in the apoAlkB spectrum. Furthermore, the binary complexes, prepared by independent addition of either Fe^{2+} or 2OG to apo protein, showed no increase in spectral dispersion (not shown). These data demonstrate that simultaneous binding of Fe^{2+} and 2OG is required for the formation of a fully folded, globular holo protein. Control experiments were performed to validate that the His$_6$-tag did not influence metal binding and/or AlkB protein folding (see Supporting Information for details).

To further assess AlkB folding, we monitored tryptophan fluorescence in the various complexes. AlkB contains four tryptophans (W11, W69, W89, and W178) that act as intrinsic reporters on (local) changes in protein folding and dynamics. Both steady-state and time-resolved fluorescence were used to examine changes in the tryptophan microenvironment. In the absence of methylated DNA, but in the presence of the cosubstrates 2OG and O_2, AlkB displays a substrate-independent background activity through which 2OG is decarboxylated to succinate.[23] To circumvent this issue, fluorescence data were collected on a holoAlkB complex binding the inhibitor NOG, a structural analogue of 2OG. The 2D ^{15}N−^{1}H HSQC spectra of AlkB-Fe^{2+}-2OG and AlkB-Fe^{2+}-NOG were alike in terms of spectral dispersion and overall chemical shifts, illustrating the structural similarities between

dx.doi.org/10.1021/bi201699e | *Biochemistry* 2012, 51, 3334−3341

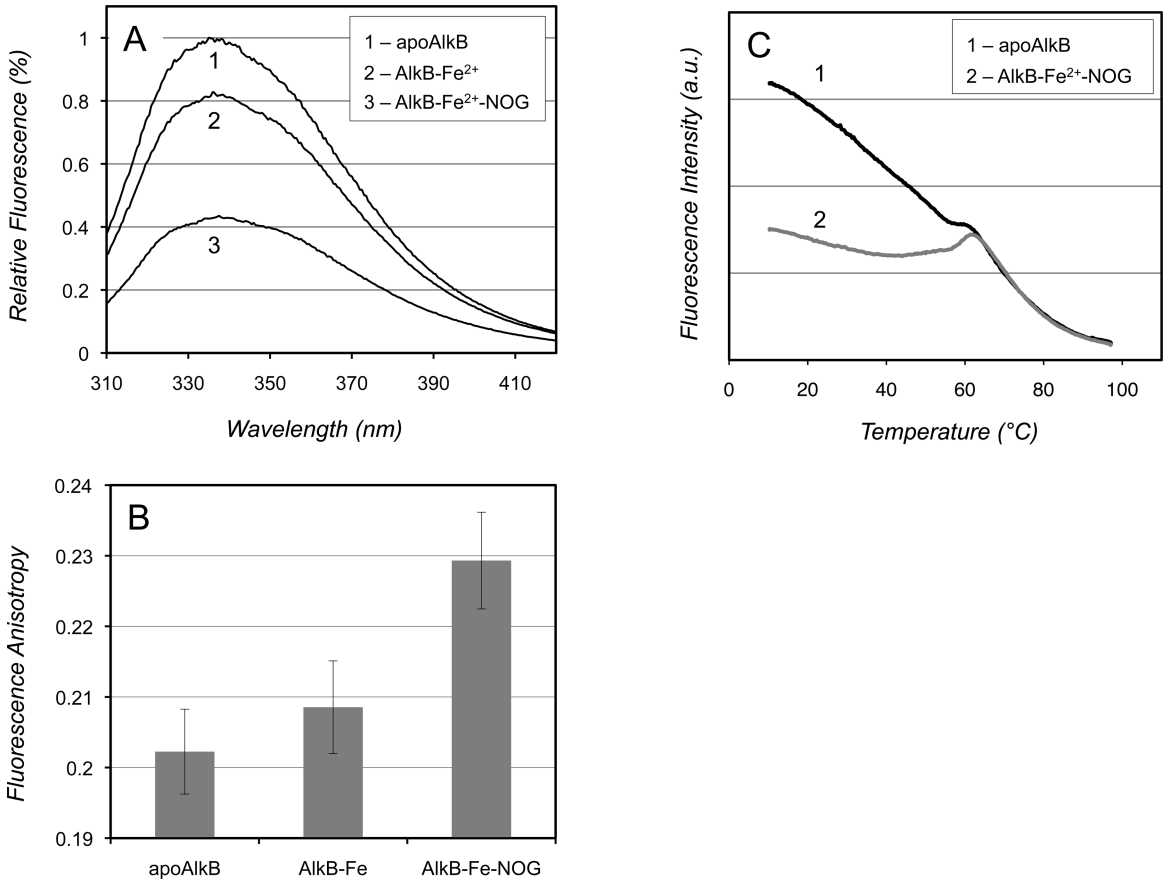

Figure 2. Equilibrium tryptophan fluorescence spectroscopy on AlkB complexes. (A) Steady-state fluorescence spectra. (B) Fluorescence anisotropy. (C) Thermal denaturation curves.

these two complexes (see Supporting Information Figure 2B for a 2D $^{15}N-^{1}H$ HSQC spectrum of the AlkB-Fe^{2+}-NOG complex).

Steady-state fluorescence spectra of apoAlkB displayed an emission band with a maximum at 343 nm typical for tryptophan residues embedded in a protein matrix (Figure 2A). Addition of Fe^{2+} to apoAlkB resulted in a drop of the fluorescence intensity to about 80%. Quenching of the fluorescence most likely results from the binding of the positive iron ion in the vicinity of W69. The fluorescence of the holoAlkB complex was much lower at only 45% of that of the apo protein. Apparently, the increased ordering of the protein's tertiary structure in the AlkB-Fe^{2+}-NOG complex leads to a more efficient quenching of the tryptophan fluorescence.

We next determined the tryptophan fluorescence anisotropy of the respective AlkB complexes (Figure 2B). Fluorescence anisotropy values for apoAlkB and the AlkB–Fe^{2+} complex were very similar at a value of 0.2. Binding of 2OG or NOG to apoAlkB in the absence of Fe^{2+} did not significantly change the fluorescence anisotropy (not shown). However, a small but clearly significant increase in anisotropy was observed after joint addition of Fe^{2+} and NOG. The anisotropy of the emitted radiation correlates with the protein microenvironment of the fluorescent tryptophan residues. Higher anisotropy indicates a decrease in mobility of the tryptophan indole side chain on the nanosecond time scale. These data therefore also point to a decrease in tryptophan side chain flexibility in holoAlkB compared to apoAlkB.

The thermal stability of the different AlkB complexes was monitored by fluorescence spectroscopy (Figure 2C). Heating caused the protein to unfold and denature, resulting in a decline in the tryptophan fluorescence intensity. ApoAlkB displayed a broad melting profile with a melting temperature T_m of ~54 °C. The largely sigmoidal profile is indicative of a single stage model describing the simple transition from a folded to an unfolded state. Subsequent cooling of the sample did not increase the signal intensity again, indicating irreversible denaturation of the protein. Binding of Fe^{2+} alone showed similar unfolding characteristics as for apoAlkB (not shown). In contrast to the apo protein, the holoAlkB complex was more resistant to thermal denaturation. Similar to before, the starting fluorescence intensity of holoAlkB was about 45% of that of apoAlkB. During the first phase (<40 °C), the relative decrease in fluorescence intensity was smaller than for apoAlkB, indicating higher stability of the holoAlkB complex. Around 40 °C the fluorescence intensity slowly started to increase to peak at 61 °C. At higher temperatures the fluorescence intensity dropped again, in parallel with the trace of the apo protein. This phenomenon is interpreted as the release of the cofactors (Fe^{2+}, NOG, or both) from the inside of the DSBH (at T_m ~ 55 °C) and a concomitant transition from the globular holo complex to the more loosely defined structure of the apo protein with a higher fluorescence intensity. These data suggest a two-stage model for unfolding of holoAlkB. In the first step the holo complex releases its cofactor(s), causing the loss of the main link between the large and the small sheet of

dx.doi.org/10.1021/bi201699e | *Biochemistry* 2012, 51, 3334–3341

the DSBH. The resulting apo-like structure then collapses to yield unfolded, denatured protein.

The effects of binding of cofactors on the tryptophan fluorescence were studied in further detail by measuring tryptophan fluorescence lifetimes. Time-dependent fluorescence decay traces were measured over a spectral range of 320 to 370 nm. To quantify the relative contributions of the fluorophores, the data were fitted using three variables. Table 1 shows the lifetime averages obtained from data fits over this spectral range (320−370 nm). Integration of the signals in the time domain and summation of the three different compounds allowed the construction of decay-associated spectra (Figure 3B−D). These decay-associated spectra can be directly compared to the steady-state fluorescence spectra. As illustrated in Figures 2 and 3, the decay-associated spectra reproduce the steady-state spectra of the various AlkB complexes very well. Individual decay traces recorded at 340 nm are shown in Figure 3A. The decrease observed in the steady-state fluorescence intensity upon binding of Fe^{2+} to apoAlkB was reflected in the different fluorescence decay traces. Fitting of the data showed a decrease of predominantly τ_2 in the AlkB−Fe^{2+} complex, resulting in a relatively small decrease (<20%) in intensity of the decay-associated spectra. This was identical to the spectrum recorded under steady-state conditions. Clearly, binding of Fe^{2+} only partially affects the fluorescence, only decreasing τ_2 without significantly changing contributions from other fluorophores.

Table 1. Tryptophan Fluorescence Lifetimes (τ, in ns) in AlkB Complexes

	τ_1	τ_2	τ_3
apoAlkB	4.86 ± 0.15	2.02 ± 0.12	0.44 ± 0.09
AlkB-Fe^{2+}	4.67 ± 0.11	1.76 ± 0.09	0.44 ± 0.05
holoAlkB	3.72 ± 0.29	1.68 ± 0.12	0.25 ± 0.03

Fluorescence decay of the holoAlkB complex again was notably different and the decay was significantly faster. This too was in agreement with the steady-state experiments where the holoAlkB complex also showed an ∼60% decrease in fluorescence intensity. In particular, the fluorophores associated with the longer lifetimes were reduced in holoAlkB (τ_1 decreased from 4.7 to 3.7 ns). As stated before, AlkB contains four tryptophan residues and a single tryptophan side chain may give rise to multiple lifetimes.[25] Therefore, the fitted data can only be used to qualitatively assess average changes in the tryptophan environment. For apoAlkB about 70% of the fluorescence intensity could be fitted using a lifetime of almost 5 ns (τ_1), which is within the normal range for tryptophan residues embedded in a protein matrix. A much smaller amount of intensity (25%) was fitted using a much shorter lifetime of 2 ns (τ_2), possibly related to more solvent exposed tryptophan residues. Finally, a small amount (5%) was fitted with a very short lifetime of 0.4 ns. Addition of Fe^{2+} to apoAlkB predominantly affected the τ_2, reducing it by ca. 20%. Subsequent addition of NOG and formation of the holoAlkB complex almost exclusively reduced the lifetime and the intensity of the fluorophores associated with τ_1. The reduced amplitude of this signal resulted in a 60% decrease in fluorescence intensity of the holo complex compared to apoAlkB.

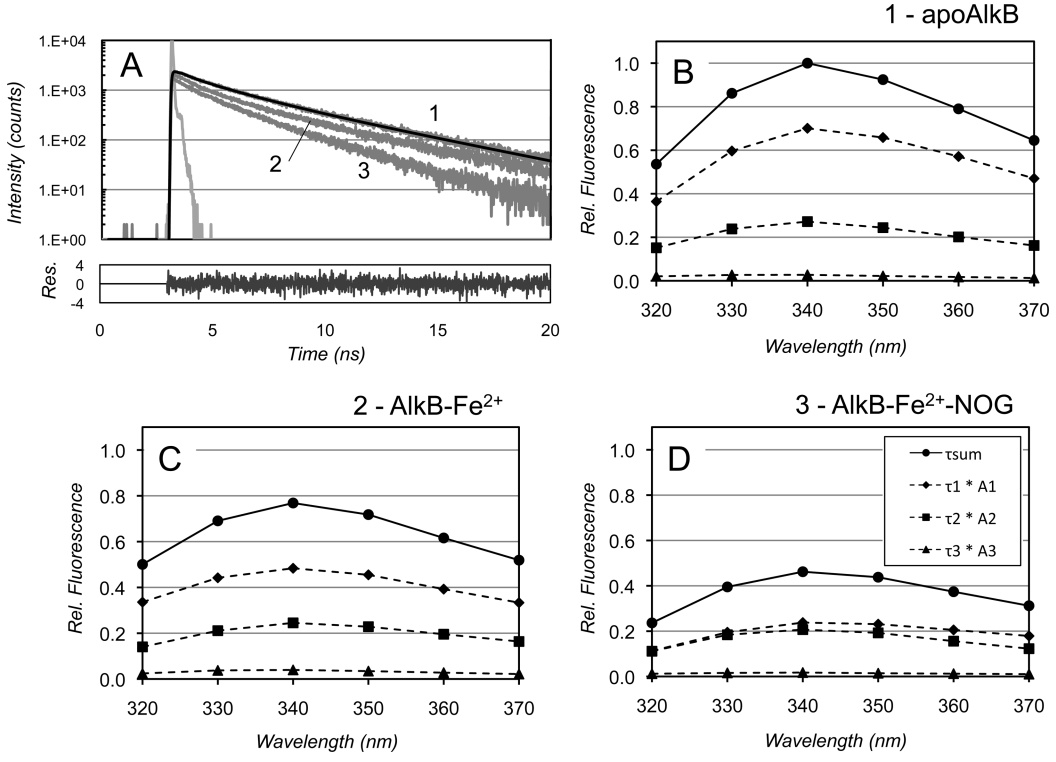

Figure 3. Tryptophan fluorescence lifetime measurements on AlkB complexes. (A) Fluorescence intensity decay traces of various AlkB complexes at 340 nm. As an example the fit and the residual of the fit is depicted for apoAlkB. (B−D) Decay associated spectra for the various AlkB complexes. Fluorescence decay traces were fitted at wavelengths ranging from 320 to 370 nm using three variables. Spectra were recorded for 120 s per wavelength and intensities are normalized to apoAlkB.

dx.doi.org/10.1021/bi201699e | *Biochemistry* 2012, 51, 3334−3341

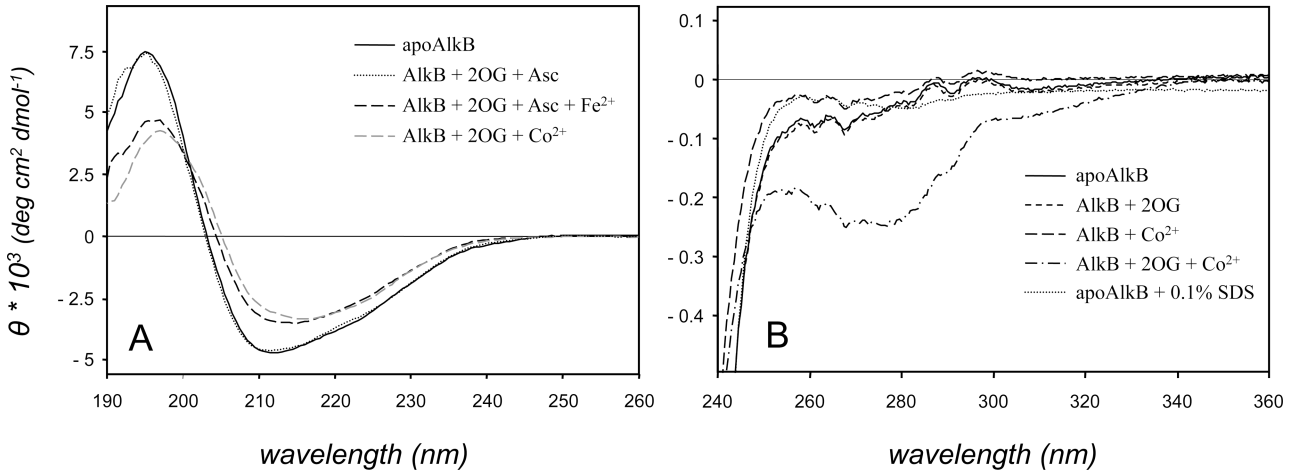

Figure 4. Binding of metal and/or 2OG to apoAlkB monitored by circular dichroism (CD) spectroscopy: (A) far-UV CD spectroscopy; (B) near-UV CD spectroscopy.

Having established that AlkB adopts different conformations in the apo and the holo state, we next assessed to what extent the two states differ in secondary structure content. To this end, far-UV CD spectra were recorded in the 190−260 nm range (Figure 4A). All complexes displayed very similar spectra, indicating that the amount of α-helical en β-sheet content is comparable in all complexes. Spectra were fitted to quantify the relative spectral contributions of helices and sheets. The results indicated that apoAlkB contained predominantly β-sheet (37%) and only a small amount (<10%) of α-helix. These values were analogous to those observed in the crystal structure of the holoAlkB complex (PDB 2FD8). Addition of metal (Fe^{2+} or Co^{2+}) to apoAlkB induced a small but reproducible change with the negative band decreasing in intensity and shifting to 215 nm. These changes correlated with a small decrease in α-helices and a slight increase in β-strands. Metal binding residues His131 and His187 are in strands βC2 and βC7 in the small β-sheet. Possibly, binding of metal induces formation or stabilization of these strands, accounting for the observed increase in β-strand content. The far-UV CD spectra of the binary AlkB−metal complexes (Fe^{2+}, Co^{2+}) were all very similar, indicating that the structural ordering is independent of the nature of the bound metal. Addition of 2OG did not induce further changes in the far-UV CD spectrum. Overall, the far-UV CD analysis showed no changes in secondary structure between apoAlkB and holoAlkB.

As a final approach to probe the effects of metal and 2OG binding on the tertiary structure, we recorded near-UV CD spectra (240−360 nm) of AlkB complexes (Figure 1B). The near-UV CD effect in proteins arises from aromatic residues and disulfide bonds. Since AlkB contains no disulfide bonds, only aromatic residues are the origin of features in the near-UV CD spectra. When proteins adopt well-folded tertiary structures the aromatic residues occupy unique environments, usually in the internal hydrophobic regions of a protein.[26] ApoAlkB showed small yet distinct features in the region between 240 and 310 nm. Two maxima between 255 and 270 nm were observed, a region in which phenylalanine residues display sharp fine structure. The maxima at 287 and 295 nm are associated with tryptophan residues. These features disappeared upon unfolding of the apo protein in 0.1% SDS (3.5 mM), demonstrating that in apoAlkB certain tryptophans occupy (partially) folded domains. Protein unfolding in SDS was confirmed by a much reduced dispersion in the amide region and the loss of upfield resonances in the methyl region of the 1D ^{1}H NMR spectrum (not shown). Independent addition of 2OG or metal to apoAlkB had no effect on the near-UV CD spectrum. In contrast, holoAlkB (AlkB-Co^{2+}-2OG) showed a distinctly different near-UV CD spectrum. In conclusion, the CD spectroscopic analysis also implies that the structural differences between apoAlkB and holoAlkB are predominantly manifest on the level of tertiary structure and protein dynamics.

■ DISCUSSION

In this study we present a biophysical characterization of AlkB, an *E. coli* DNA repair protein and 2OG-dependent dioxygenase. Our results indicate that AlkB adopts significantly different structures in solution. HoloAlkB binds both Fe^{2+} and 2OG and shows all the characteristics of a well-folded globular protein. However, apoAlkB is a flexible protein that samples multiple conformations on an intermediate NMR time scale (millisecond to microsecond). This results in severely broadened resonances, often beyond detection. The resolved residues in apoAlkB predominantly map to the two N-terminal helices (αN1 and αC1) that support the DSBH catalytic core and the βL1 strand adjacent to the large β-sheet. Resonances from the central parts of the large and the small β-sheets were not observed in the $^{1}H-^{15}N$ HSQC spectrum of apoAlkB. Both fluorescence and near-UV CD spectroscopy data support the notion that apoAlkB is a highly dynamic protein. Far-UV CD spectra indicate however that on the level of secondary structure the differences between apoAlkB and holoAlkB are minimal.

Examination of the AlkB crystal structures demonstrates that the DSBH core contains only few intersheet contacts, besides the indirect ones via 2OG and Fe^{2+}. In the absence of cofactors the DSBH cannot be stabilized by intersheet contacts. We therefore postulate that in apoAlkB the DSBH core is dynamic and experiences severe conformational exchange. We have previously identified similar dynamic behavior, albeit to a much lesser extent, for AlkB in a succinate-bound state.[18] Binding of succinate to the core of AlkB increased the protein flexibility compared to binding of 2OG. Similar protein dynamics has previously been observed for the catalytic domain of PHD2, a 2OG dioxygenase involved in oxygen sensing.[18,27] In AlkB, mutagenesis of asparagine at position 120 to alanine further

dx.doi.org/10.1021/bi201699e | *Biochemistry* 2012, 51, 3334−3341

showed that this residue is important to maintain the fold of the holo protein. Asparagine 120 is located at the bottom of the large β-sheet in the C1 β-strand. It lines the back of the cosubstrate binding cavity and forms a hydrogen bond with the 1-carboxylic group of 2OG via its side chain $-NH_2$ moiety. Mutagenesis to alanine prevented the formation of this contact and resulted in a flexible complex, also when 2OG was bound. We concluded that a dynamic DSBH core is required for the release of succinate from the inside of the protein after catalysis.

In light of our current findings, we propose a two-stage model for the folding of holoAlkB. The unfolded protein initially folds into a partially structured apoAlkB. This state can bind the required cofactors to fold into a globular holoAlkB complex. Such a model is supported by the thermal unfolding studies presented in Figure 2C which mirror the kinetics of the proposed two-stage folding model. This model involves an apo protein that already contains the secondary structure elements (i.e., sheets and helices). However, these structured elements and linking regions exhibit a degree of disorder and dynamics, very similar to those observed in molten globules in which the lack of native tertiary interactions results in an ensemble of conformations. Independent binding of 2OG or Fe^{2+} to apoAlkB has negligible effect on tertiary structure, as shown by NMR and near-UV CD spectroscopy. However, synchronized binding of 2OG (or NOG) and Fe^{2+} facilitates the requisite contacts between the small and large β-sheets to form the canonical DSBH core characteristic for the family of 2OG dioxygenases.

Analysis of the available crystal structures for the members of this subfamily of 2OG dioxygenases shows that the contact between the asparagine side chain and 2OG is strictly conserved. This contact provides the main link between the major and the minor sheet of the DSBH via 2OG and Fe^{2+}. All crystal structures of human AlkB homologues (ABH) resolved to date contain an asparagine residue in the C1 β-strand of the large β-sheet: N159 in ABH2 (PDB 3BU0), N179 in ABH3 (2IUW), N227 in ABH8 (3THP), and N205 in FTO (3LFM). For structures see also Supporting Information, Figure 3. The structures of holo ABH complexes further show that the cosubstrate 2OG is buried in the interior of the protein, similar to the positioning in AlkB. In view of the structural homologies we hypothesize that the human proteins display dynamic characteristics similar to AlkB and that protein dynamics is required for adequate (co)substrate binding and release during catalysis. Biophysical analyses of the human AlkB homologues are currently carried out in our laboratories.

In conclusion, our data indicate that AlkB is an intrinsically flexible protein adopting different folding states in the apo and the holo form. These observations are in line with a previous study that showed AlkB is a dynamic protein that adopts different conformations and dynamics dependent on whether 2OG or succinate is bound in the active site.[18] It was postulated that the plasticity of AlkB (1) facilitates the binding of 2OG and the release of succinate from the protein's interior during catalysis and (2) is required for the efficient binding and release of DNA bases during repair. At this stage it is not clear how AlkB is able to rapidly scan DNA to efficiently identify and repair methyl lesions. Affinity measurements showed that apoAlkB binds ssDNA with an ~50-fold lower affinity than the holo complex. However, at this stage we have no experimental evidence indicating that the apo state of AlkB is part of the catalytic cycle and/or directly involved in lesion detection.

Recent studies have shown that Fe^{2+} incorporation into the 2OG dioxygenases, PHD and FIH, is an active process that requires the iron chaperones PCBP1 and PCBP2.[28] The Fe^{2+}-binding proteins PCBP1 and PCBP2 interact with PHD and FIH and are thought to deliver the metal to the active site of these dioxygenases. It has previously been shown that the PHD dioxygenase is a dynamic protein, similar to AlkB.[18,27] A role for PCBP1 and PCBP2 in metalation of the mammalian homologues of AlkB (ABH1−8 and FTO) has also been proposed.[28] A plausible scenario for the formation of active 2OG dioxygenases in mammalian cells would be the following: after translation, 2OG dioxygenases initially fold into adaptable apo proteins, similar to observed here for apoAlkB. The Fe^{2+} chaperone (PCBP1 and/or PCBP2) then interacts with the dynamic apo protein and delivers the Fe^{2+} ion to the 2OG dioxygenase active site. Binding of metal, and subsequently of the cofactor 2OG, promotes complete folding and formation of a globular holo protein. An attractive hypothesis would be that Fe^{2+} chaperones bind preferentially to apo 2OG dioxygenases. After delivery of the Fe^{2+} ion, the reduced protein dynamics of the globular holo 2OG dioxygenase might result in a much lower binding affinity for the Fe^{2+} chaperones. This would provide an elegant mechanism to modulate the interactions between the Fe^{2+} chaperones and their target 2OG dioxygenases via protein dynamics.

■ ASSOCIATED CONTENT

Supporting Information

A detailed description of the AlkB protein constructs used in this study; SDS-PAGE analysis of purified AlkB proteins (Figure S1); $^{15}N-^{1}H$ HSQC NMR spectra of an AlkB construct without a His6-tag (Figure S2); a structural comparison of the 2OG binding site in mammalian 2OG dioxygenases (Figure S3). This material is available free of charge via the Internet at http://pubs.acs.org.

■ AUTHOR INFORMATION

Corresponding Author

*Tel +31 20 5665131, e-mail b.bleijlevens@amc.uva.nl (B.B.); Tel +44 207 5945315, e-mail s.j.matthews@imperial.ac.uk (S.J.M.).

Funding

This research was supported by Cancer Research UK grant C16554 and the BBSRC. Acquisition of the Chirascan CD spectrometer was supported by BBSRC Grant BB/C510859/1.

Notes

The authors declare no competing financial interest.

■ ACKNOWLEDGMENTS

A subset of the NMR spectra were recorded on a 600 MHz Bruker Avance NMR spectrometer at the SONNMRLSF in Utrecht, The Netherlands. The assistance of Dr. Hans Wienk with these experiments is greatly appreciated. We thank Dr. Barbara Sedgwick for her interest in our study and comments on an initial version of this manuscript. Drs. Noam Zelcer, Dave Speijer, and Rozemarijn van Duursen are acknowledged for critical reading of the manuscript, suggestions, and comments.

■ ABBREVIATIONS

2OG, 2-oxoglutarate; NOG, *N*-oxalylglycine; DSBH, double-stranded β-helix; ABH, α-ketoglutarate-dependent dioxygenase AlkB homologue.

REFERENCES

(1) Sedgwick, B. (2004) Repairing DNA-methylation damage. *Nat. Rev. Mol. Cell Biol. 5*, 148−157.

(2) Rose, N. R., McDonough, M. A., King, O. N. F., Kawamura, A., and Schofield, C. J. (2011) Inhibition of 2-oxoglutarate dependent oxygenases. *Chem. Soc. Rev. 40*, 4364−4397.

(3) Falnes, P., Johansen, R. F., and Seeberg, E. (2002) AlkB-mediated oxidative demethylation reverses DNA damage in Escherichia coli. *Nature 419*, 178−182.

(4) Trewick, S. C., Henshaw, T. F., Hausinger, R., Lindahl, T., and Sedgwick, B. (2002) Oxidative demethylation by Escherichia coli AlkB directly reverts DNA base damage. *Nature 419*, 174−178.

(5) Aas, P. A., Otterlei, M., Falnes, P. O., Vagbo, C. B., Skorpen, F., Akbari, M., Sundheim, O., Bjoras, M., Slupphaug, G., Seeberg, E., and Krokan, H. E. (2003) Human and bacterial oxidative demethylases repair alkylation damage in both RNA and DNA. *Nature 421*, 859−863.

(6) Ougland, R., Zhang, C. M., Liiv, A., Johansen, R. F., Seeberg, E., Hou, Y. M., Remme, J., and Falnes, P. O. (2004) AlkB restores the biological function of mRNA and tRNA inactivated by chemical methylation. *Mol. Cell 16*, 107−116.

(7) Sedgwick, B., Bates, P., Paik, J., Jacobs, S., and Lindahl, T. (2007) Repair of alkylated DNA: Recent advances. *DNA Repair 6*, 429−442.

(8) Duncan, T., Trewick, S. C., Koivisto, P., Bates, P. A., Lindahl, T., and Sedgwick, B. (2002) Reversal of DNA alkylation damage by two human dioxygenases. *Proc. Natl. Acad. Sci. U. S. A. 99*, 16660−16665.

(9) Westbye, M. P., Feyzi, E., Aas, P. A., Vagbo, C. B., Talstad, V. A., Kavli, B., Hagen, L., Sundheim, O., Akbari, M., Liabakk, N. B., Slupphaug, G., Otterlei, M., and Krokan, H. E. (2008) Human AlkB homolog 1 is a mitochondrial protein that demethylates 3-methylcytosine in DNA and RNA. *J. Biol. Chem. 283*, 25046−25056.

(10) Songe-Moller, L., van den Born, E., Leihne, V., Vagbo, C. B., Kristoffersen, T., Krokan, H. E., Kirpekar, F., Falnes, P. O., and Klungland, A. (2010) Mammalian ALKBH8 Possesses tRNA Methyltransferase Activity Required for the Biogenesis of Multiple Wobble Uridine Modifications Implicated in Translational Decoding. *Mol. Cell. Biol. 30*, 1814−1827.

(11) Frayling, T. M., Timpson, N. J., Weedon, M. N., Zeggini, E., Freathy, R. M., Lindgren, C. M., Perry, J. R., Elliott, K. S., Lango, H., Rayner, N. W., Shields, B., Harries, L. W., Barrett, J. C., Ellard, S., Groves, C. J., Knight, B., Patch, A. M., Ness, A. R., Ebrahim, S., Lawlor, D. A., Ring, S. M., Ben-Shlomo, Y., Jarvelin, M. R., Sovio, U., Bennett, A. J., Melzer, D., Ferrucci, L., Loos, R. J., Barroso, I., Wareham, N. J., Karpe, F., Owen, K. R., Cardon, L. R., Walker, M., Hitman, G. A., Palmer, C. N., Doney, A. S., Morris, A. D., Smith, G. D., Hattersley, A. T., and McCarthy, M. I. (2007) A common variant in the FTO gene is associated with body mass index and predisposes to childhood and adult obesity. *Science 316*, 889−894.

(12) Jia, G., Yang, C., Yang, S., Jian, X., Yi, C., Zhou, Z., and He, C. (2008) Oxidative demethylation of 3-methylthymine and 3-methyluracil in single-stranded DNA and RNA by mouse and human FTO. *FEBS Lett. 582*, 3313−3319.

(13) Gerken, T., Girard, C. A., Tung, Y. C., Webby, C. J., Saudek, V., Hewitson, K. S., Yeo, G. S., McDonough, M. A., Cunliffe, S., McNeill, L. A., Galvanovskis, J., Rorsman, P., Robins, P., Prieur, X., Coll, A. P., Ma, M., Jovanovic, Z., Farooqi, I. S., Sedgwick, B., Barroso, I., Lindahl, T., Ponting, C. P., Ashcroft, F. M., O'Rahilly, S., and Schofield, C. J. (2007) The obesity-associated FTO gene encodes a 2-oxoglutarate-dependent nucleic acid demethylase. *Science 318*, 1469−1472.

(14) Yu, B., Edstrom, W., Benach, J., Hamuro, Y., Weber, P., Gibney, B., and Hunt, J. (2006) Crystal structures of catalytic complexes of the oxidative DNA/RNA repair enzyme AlkB. *Nature 439*, 879−884.

(15) Yang, C., Yi, C., Duguid, E., Sullivan, C., Jian, X., Rice, P., and He, C. (2008) Crystal structures of DNA/RNA repair enzymes AlkB and ABH2 bound to dsDNA. *Nature 452*, 961−965.

(16) Sundheim, O., Vågbø, C., Bjørås, M., Sousa, M., Talstad, V., Aas, P., Drabløs, F., Krokan, H., Tainer, J., and Slupphaug, G. (2006) Human ABH3 structure and key residues for oxidative demethylation to reverse DNA/RNA damage. *EMBO J. 25*, 3389−3397.

(17) Pastore, C., Topalidou, I., Forouhar, F., Yan, A. C., Levy, M., and Hunt, J. F. (2012) Crystal structure and RNA binding properties of the RRM/AlkB domains in human ABH8, an enzyme catalyzing tRNA hypermodification. *J. Biol. Chem. 287*, 2130−2143.

(18) Bleijlevens, B., Shivarattan, T., Flashman, E., Yang, Y., Simpson, P. J., Koivisto, P., Sedgwick, B., Schofield, C. J., and Matthews, S. J. (2008) Dynamic states of the DNA repair enzyme AlkB regulate product release. *EMBO Rep. 9*, 872−877.

(19) Clifton, I. J., McDonough, M. A., Ehrismann, D., Kershaw, N. J., Granatino, N., and Schofield, C. J. (2006) Structural studies on 2-oxoglutarate oxygenases and related double-stranded beta-helix fold proteins. *J. Inorg. Biochem. 100*, 644−669.

(20) Bleijlevens, B., Shivarattan, T., Sedgwick, B., Rigby, S. E., and Matthews, S. J. (2007) Replacement of non-heme Fe(II) with Cu(II) in the alpha-ketoglutarate dependent DNA repair enzyme AlkB: spectroscopic characterization of the active site. *J. Inorg. Biochem. 101*, 1043−1048.

(21) Smoluch, M., Joshi, H., Gerssen, A., Gooijer, C., and van der Zwan, G. (2005) Fast excited-state intramolecular proton transfer and subnanosecond dynamic stokes shift of time-resolved fluorescence spectra of the 5-methoxysalicylic acid/diethyl ether complex. *J. Phys. Chem. A 109*, 535−541.

(22) Whitmore, L., and Wallace, B. A. (2004) DICHROWEB, an online server for protein secondary structure analyses from circular dichroism spectroscopic data. *Nucleic Acids Res. 32*, W668−673.

(23) Henshaw, T. F., Feig, M., and Hausinger, R. (2004) Aberrant activity of the DNA repair enzyme AlkB. *J. Inorg. Biochem. 98*, 856−861.

(24) Shivarattan, T., Chen, H., Simpson, P., Sedgwick, B., and Matthews, S. (2005) Resonance assignments of Escherichia coli AlkB: a key 2-oxoglutarate and Fe(II) dependent dioxygenase of the adaptive DNA-repair response. *J. Biomol. NMR 33*, 138.

(25) Lakowicz, J. R. (2006) *Principles of Fluorescence Spectroscopy*, 3rd ed., Springer, Berlin.

(26) Kelly, S. M., and Price, N. C. (2000) The use of circular dichroism in the investigation of protein structure and function. *Curr. Protein Pept. Sci. 1*, 349−384.

(27) Stubbs, C. J., Loenarz, C., Mecinovic, J., Yeoh, K. K., Hindley, N., Lienard, B. M., Sobott, F., Schofield, C. J., and Flashman, E. (2009) Application of a proteolysis/mass spectrometry method for investigating the effects of inhibitors on hydroxylase structure. *J. Med. Chem. 52*, 2799−2805.

(28) Nandal, A., Ruiz, J. C., Subramanian, P., Ghimire-Rijal, S., Sinnamon, R. A., Stemmler, T. L., Bruick, R. K., and Philpott, C. C. (2011) Activation of the HIF prolyl hydroxylase by the iron chaperones PCBP1 and PCBP2. *Cell Metab. 14*, 647−657.